Electronic Supplementary Information

Experimental Section

Materials: Zirconium dioxide (ZrO_2, 99.99%) was purchased from MACKLIN. Hydrochloric acid (HCl, 99.0%), ammonium chloride (NH_4Cl), sodium hypochlorite solution (NaClO), sodium citrate dehydrate ($C_6H_5Na_3O_7 \cdot 2H_2O$), salicylic acid ($C_7H_6O_3$), *p*-dimethylaminobenzaldehyde ($C_9H_{11}NO$) and sodium nitroferricyanide dihydrate ($C_5FeN_6Na_2O \cdot 2H_2O$) were purchased from Aladdin Ltd. (Shanghai, China). Nafion (5 wt%) solution was purchased from Sigma-Aldrich Chemical Reagent Co., Ltd. Hydrochloric acid (HCl), sulfuric acid (H_2SO_4), hydrogen peroxide (H_2O_2), hydrazine monohydrate ($N_2H_4 \cdot H_2O$) and ethyl alcohol (C_2H_5OH) were purchased from Beijing Chemical Corp. (China). chemical Ltd. in Chengdu. The ultrapure water used throughout all experiments was purified through a Millipore system. All reagents were analytical reagent grade without further purification.

Characterizations: Power XRD data were acquired by a LabX XRD-6100 X-ray diffractometer with a Cu Kα radiation (40 kV, 30 mA) of wavelength 0.154 nm (SHIMADZU, Japan). TEM images were acquired on a HITACHI H-8100 electron microscopy (Hitachi, Tokyo, Japan) operated at 200 kV. XPS measurements were performed on an ESCALABMK II X-ray photoelectron spectrometer using Mg as the exciting source. The absorbance data of spectrophotometer was measured on UV-Vis spectrophotometer.

Preparation of ZrO_2/CP: 10 mg catalyst was grinded into powder and mixed with 1 mL of ethonal containing Nafion solution (5%) followed by 30 min ultrasonic dispersion to form a homogeneous suspension. 10 μL of such suspension was then dropped on a 1 cm^2 carbon paper and dried ambiently. The loading mass of electrocatalysts is 0.1 mg.

Electrochemical measurements: In this paper, we use a H-type electrolytic cell separated by a Nafion Membrane which was protonated by boiling in ultrapure water, H_2O_2 (5%) aqueous solution and 0.5 M H_2SO_4 at 80 °C for another 2 h, respectively. A three-electrode configuration is used for electrochemical experiments which the catalyst coated carbon paper as the working electrode, the Ag/AgCl/saturated KCl is the reference electrode and graphite rod as the counter electrode. The electrochemical experiments were carried out with an electrochemical workstation (CHI 660E) in N_2-saturated 0.1 M HCl solution. The potentials reported in this work were converted to reversible hydrogen electrode (RHE) scale via calibration with the following equation: E (RHE) = E (vs. Ag/AgCl) + 0.256 V and the presented current density was normalized to the geometric surface area.

Determination of NH_3: The NH_3 produced by the reaction was detected with indophenol blue indicator by UV-Vis spectroscopy. [1] In 0.1M HCl, firstly, 2 mL of the electrolyte taken from cathode was mixed with 2 mL 1 M NaOH containing 5% sodium citrate and 5% salicylic acid. Then, 1 mL 0.05 M NaClO was added into such mixed solution. Finally, 0.2 mL 1% $C_5FeN_6Na_2O$ was added. After standing for 2h without exposure, such solution was identified via UV-Vis spectroscopy at the wavelength of 655 nm. The fitting curve ($y = 0.36919x + 0.0417$, $R^2 = 0.999$) shows good linear relation of absorbance value with NH_3 concentration.

Determination of N_2H_4: The N_2H_4 production was estimated by the method of Watt and Chrisp.[2] The color reagent was a mixed solution of 5.99 g $C_9H_{11}NO$, 30 mL HCl and 300 mL C_2H_5OH. In detail, 5 mL electrolyte was removed from the electrochemical reaction vessel, and added into 5 mL prepared color reagent and stirred 15 min at 25 °C. The absorbance of such solution at the absorbance of 455 nm was measured to quantify the hydrazine yields with a standard curve of hydrazine ($y = 0.76267x+0.0496$, $R^2 = 0.998$).

Determination of FE and V_{NH3}: The FE was calculated by equation:

$$FE = 3F \times c_{NH3} \times V / 17 \times Q$$

NH_3 yield was calculated using the following equation:

$$V_{NH3} = (c_{NH3} \times V) / (17 \times m_{cat.})$$

The amount of NH_3 was calculated as follows:

$$m_{NH3} = [NH_3] \times V$$

Where F is the Faraday constant, c_{NH3} is the measured NH_3 concentration, V is the volume of the HCl electrolyte for NH_3 collection, and t is the reduction time and $m_{cat.}$ is the catalyst mass.

DFT calculation details: The spin-polarized DFT calculations have been performed by using the Vienna ab initio simulation package (VASP) with the projected augment wave (PAW) pseudopotential[3,4] and the Perdew, Burke, and Ernzerhof (PBE) functional.[5] The weak van der Waals (vdW) interactions were described by the DFT+D3 method.[6] The plane-wave basis set has been used with the kinetic cutoff energy of 450 eV. The convergence criteria for the total energy and the Hellmann-Feynman force were 10^{-5} eV and 0.02 eVÅ^{-1}, respectively. The ZrO_2 (-111) (2×2) supercell was studied with a vacuum layer of ~ 15 Å. For such supercell, 2×2×1 Monkhorst-Pack grids[7] were used for the structural optimization. The calculations of the Gibbs free-energy change for each elemental step have adopted the computational hydrogen electrode model proposed by Nørskov et al.,[8] which can be obtained by the following equation

$$\Delta G = \Delta E + \Delta E_{ZPE} - T\Delta S + eU$$

The relevant total energy (E), zero-point energy (E_{ZPE}), and entropy (S) of the adsorbed intermediates were obtained from DFT calculations (Table S2), while the thermodynamic corrections for the free molecules were taken from the NIST databases.[9]

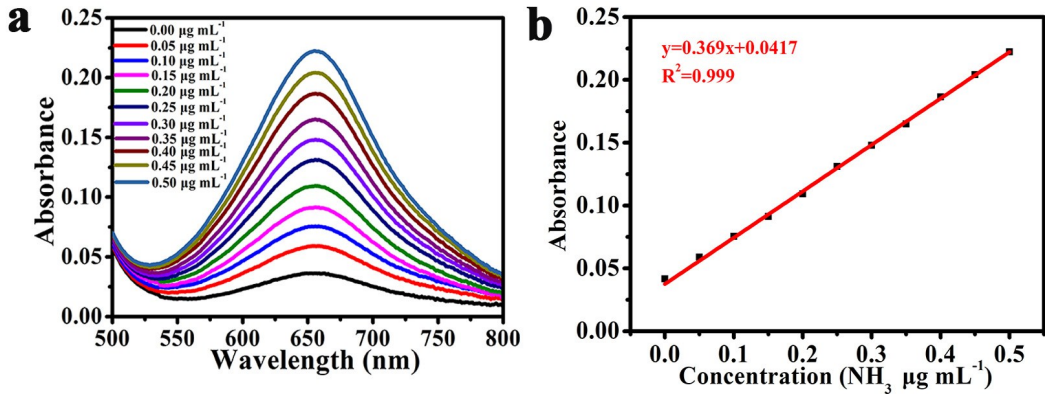

Fig. S1.

(a) UV-Vis absorption curves of indophenol assays kept with different concentrations of NH_4^+ ions for 2 h at room temperature. (b) A calibration curve used to estimate the concentration of NH_4^+concentration.

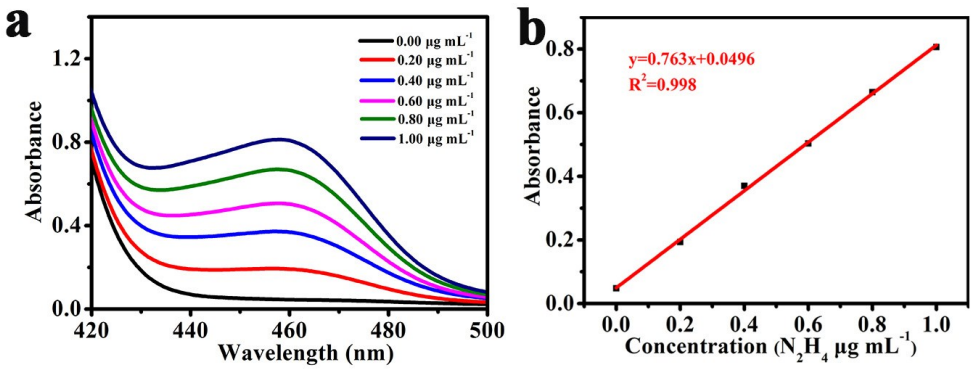

Fig. S2. (a) UV-Vis curves of various N_2H_4 concentrations after incubated for 15 min at room temperature. (b) Calibration curve used for calculation of N_2H_4 concentrations.

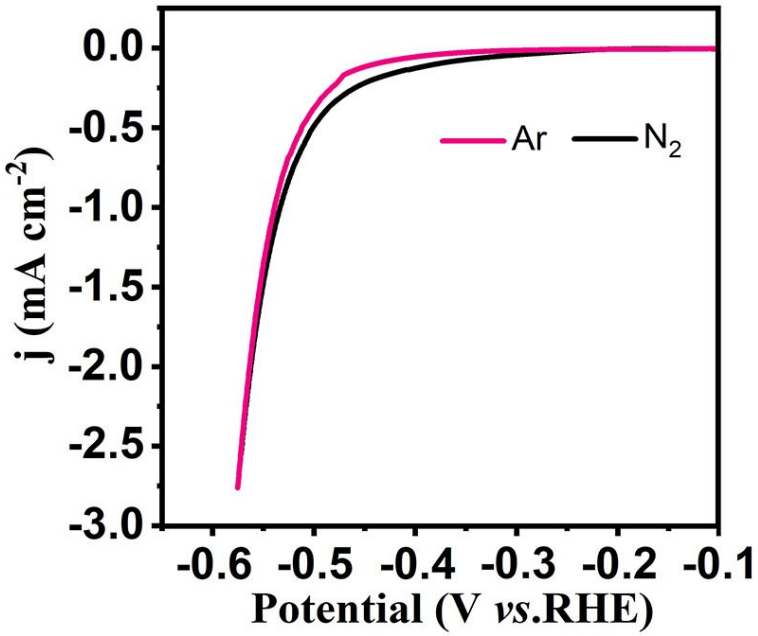

Fig. S3. LSV curves of ZrO_2/CP electrolytes in N_2- and Ar-saturated 0.1 M HCl electrolytes with a scan rate of 5 mV s^{-1}.

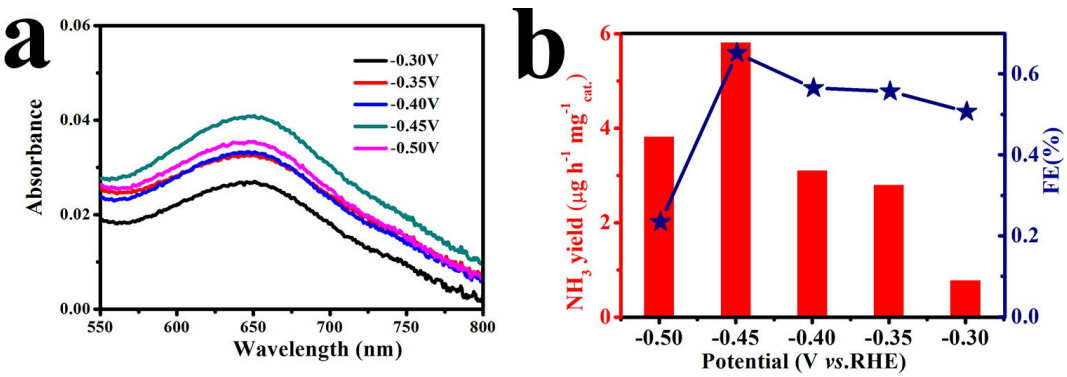

Fig. S4. (a) UV-Vis absorption spectra of the electrolytes stained with indophenol indicator after electrolysis at a series of potentials in 0.2 M PBS. (b) Average NH_3 yields and FEs for ZrO_2/CP at each given potential.

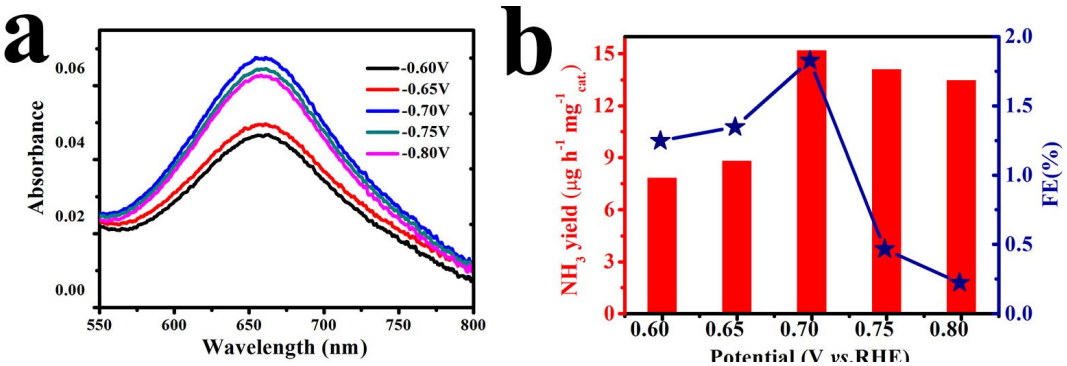

Fig. S5. (a) UV-Vis absorption spectra of the electrolytes stained with indophenol indicator after electrolysis at a series of potentials in 0.1 M KOH. (b) Average NH_3 yields and FEs for ZrO_2/CP at each given potential.

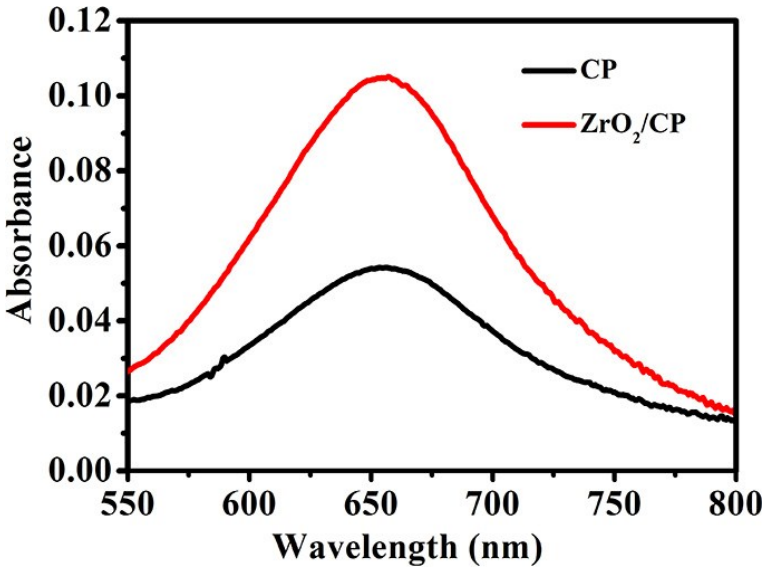

Fig. S6. UV-Vis absorption spectra of indophenol assays with ZrO_2/CP and blank CP at -0.45 V in N_2-saturated 0.1 M HCl.

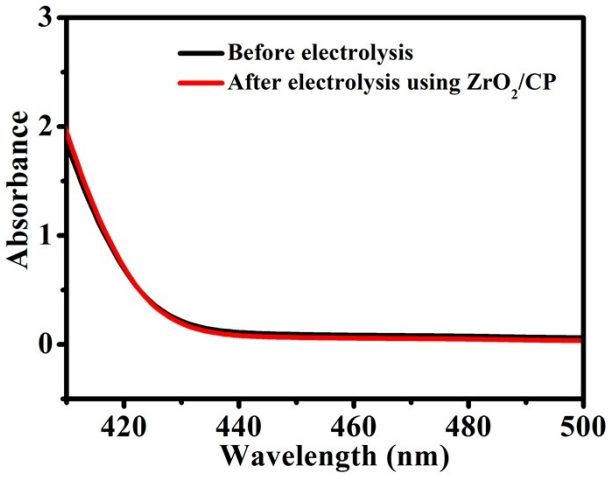

Fig. S7. UV-Vis absorption spectra of the electrolytes estimated by the method of Watt and Chrisp before and after 2 h electrolysis in N_2 atmosphere at –0.45 V.

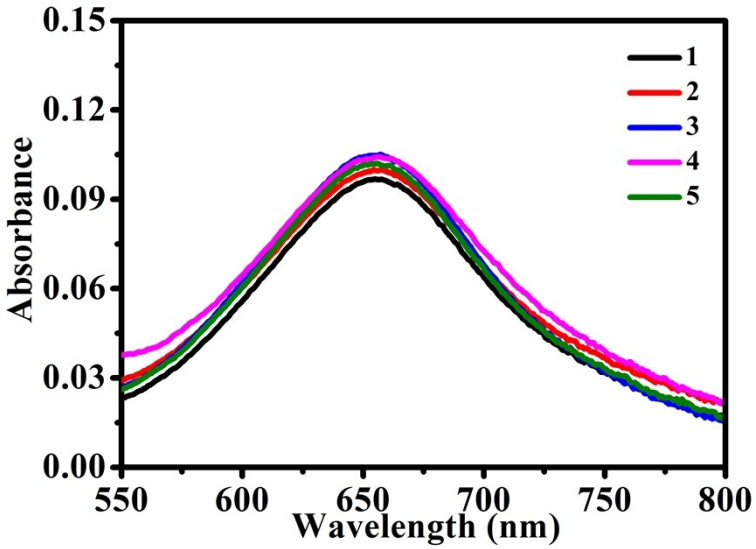

Fig. S8. UV-Vis absorption spectra of the electrolytes stained with indophenol indicator after 2 h NRR electrolysis at -0.45 V over 5 cycles.

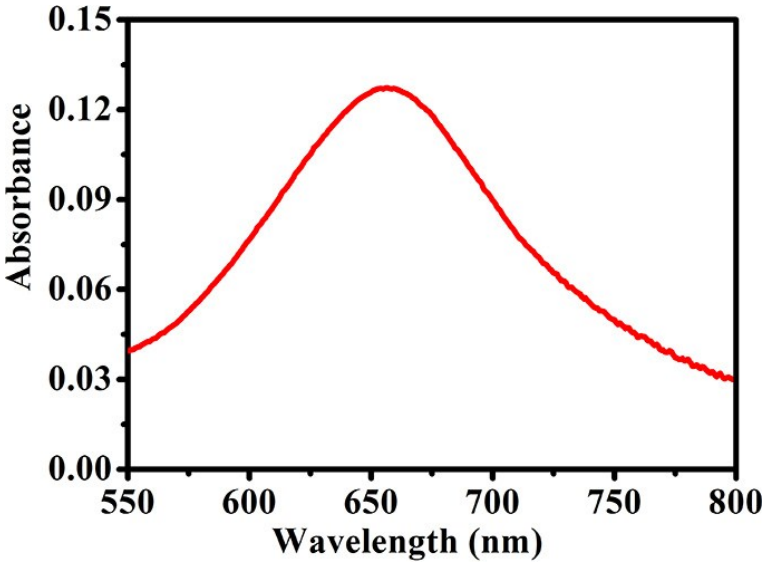

Fig. S9. UV-Vis absorption spectrum of the electrolyte stained with indophenol indicator after electrolysis at −0.45 V for 24 h.

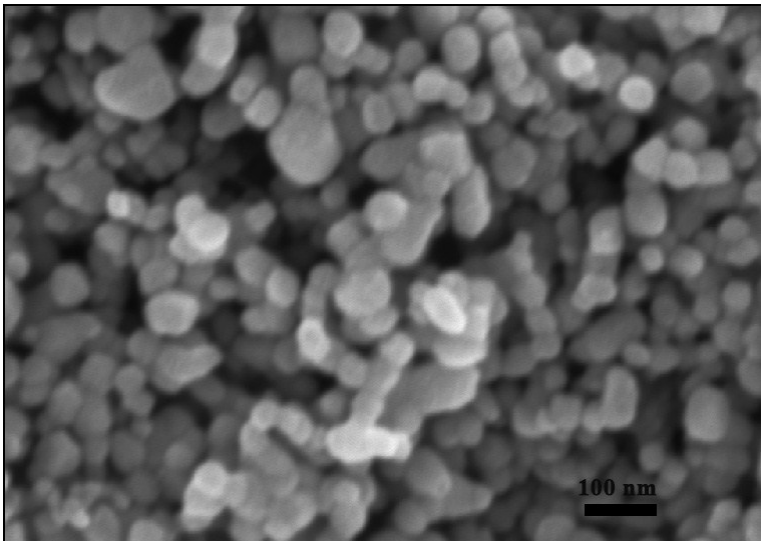

Fig. S10. SEM image for ZrO_2 nanoparticles after stability test.

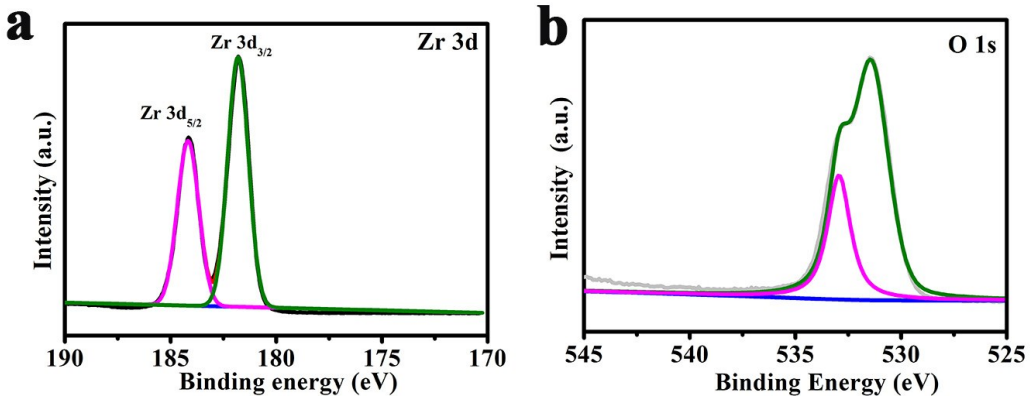

Fig. S11. The Zr 3d (a) and O 1s (b) XPS spectra of ZrO_2 after stability test.

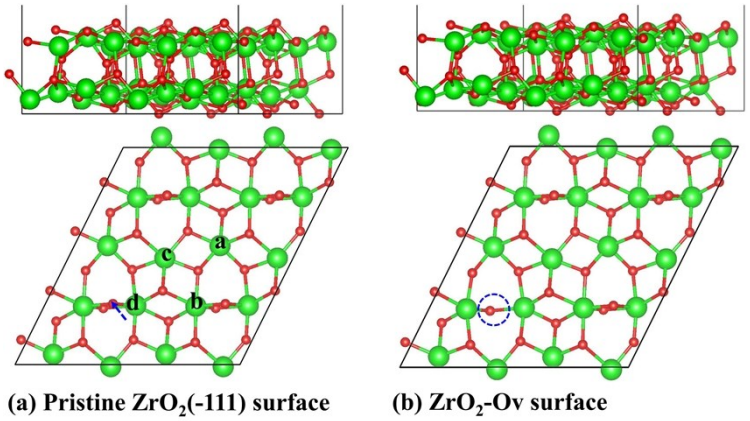

Fig. S12. The side and top views of the pristine ZrO_2 (-111) (a) and ZrO_2-Ov (b) surfaces. The ZrO_2 (-111) surface slab model contains six atomic layers, in which the bottom three layers are fixed to mimic the bulk. In (a), the four different Zr atoms on the surface are marked with a, b, c, and d. In (b), the rough position of the O vacancy is enclosed by a dashed circle. In addition, for clarity, only the first three atomic layers for the top views are displayed.

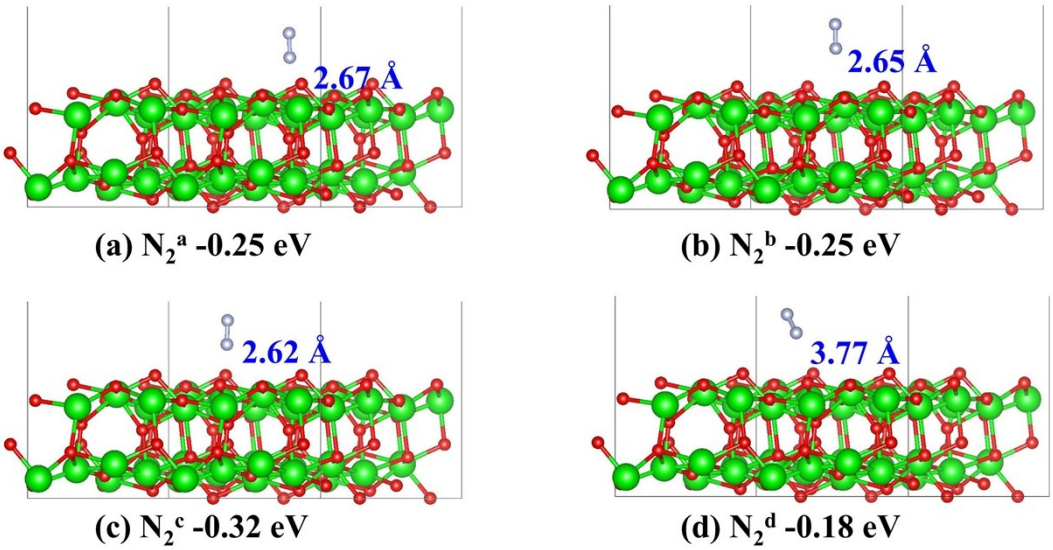

Fig. S13. The side views of the most stable configuration for the N_2 adsorption on the four sites shown in Fig. S12a of the pristine ZrO_2 (-111) surface. The adsorption energies and the nearest distances between the N_2 molecule and the surface Zr atoms are given.

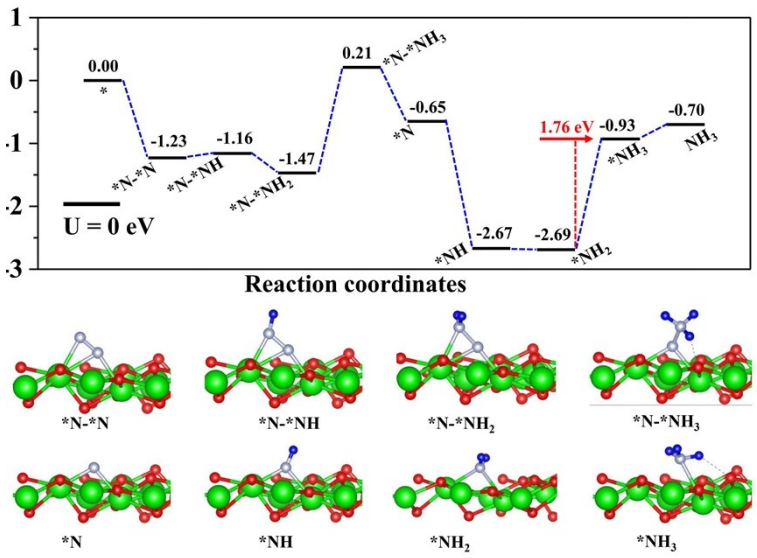

Fig. S14. The free energy (in eV) diagrams and the local atomic structures of the reaction intermediates for NRR on the ZrO_2-Ov surface at zero potential along the consecutive pathway.

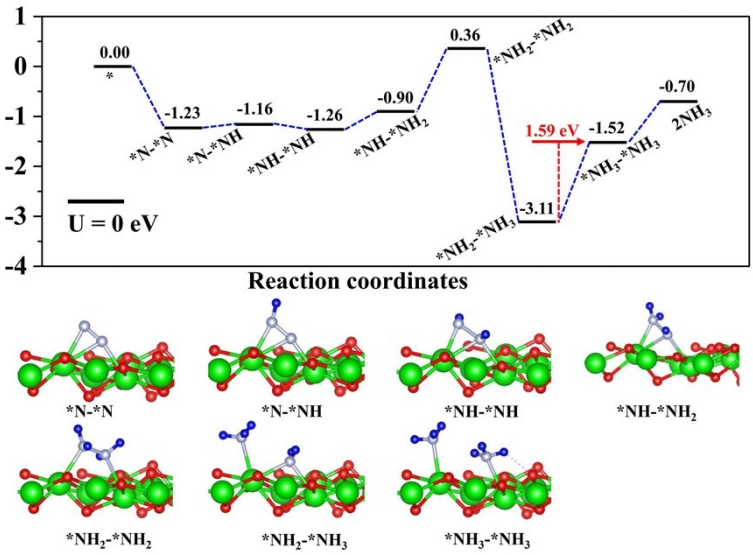

Fig. S15. The free energy (in eV) diagrams and the local atomic structures of the reaction intermediates for NRR on the ZrO_2-Ov surface at zero potential along the enzymatic pathway.

Table S1. Comparison of electrocatalytic NRR performance for ZrO_2 with other electrocatalysts under ambient conditions.

Catalyst	Electrolyte	NH_3 yield	FE (%)	Ref.
ZrO_2 /CP	0.1 M HCl	24.74 μg h^{-1} $mg^{-1}_{cat.}$	5.0	This work
Fe_2O_3-CNT	$KHCO_3$	0.22 μg h^{-1} cm^{-2}	0.15	10
Fe_2O_3 nanorods	0.1 M Na_2SO_4	15.9 μg h^{-1} $mg^{-1}_{cat.}$	0.94	11
Fe_3O_4 nanorod	0.1 M Na_2SO_4	5.6×10^{-11} mol s^{-1} cm^{-2}	2.6	12
TiO_2 nanosheets array	0.1 M Na_2SO_4	9.16×10^{-11} mol $s^{-1} \cdot cm^{-2}$	2.5	13
TiO_2-rGO	0.1 M Na_2SO_4	15.13 μg h^{-1} $mg^{-1}_{cat.}$	3.3	14
CuO/rGO	0.1 M Na_2SO_4	1.8×10^{-10} mol s^{-1} cm^{-2}	3.9	15
r-CeO_2 nanorod	0.1 M Na_2SO_4	16.4 μg h^{-1} $mg^{-1}_{cat.}$	3.7	16
MnO	0.1 M Na_2SO_4	7.92 μg h^{-1} $mg^{-1}_{cat.}$	8.02	17
Mn_3O_4-rGO	0.1 M Na_2SO_4	17.4 μg h^{-1} $mg^{-1}_{cat.}$	3.52	18
Mn_3O_4 nanocube	0.1 M Na_2SO_4	11.6 μg h^{-1} $mg^{-1}_{cat.}$	3.0	19
SnO_2	0.1 M Na_2SO_4	5.6×10^{-11} mol s^{-1} cm^{-2}	2.17	20
SnO_2/rGO	0.1 M Na_2SO_4	25.6 μg h^{-1} $mg^{-1}_{cat.}$	7.1	21
F-SnO_2 nanosheet	0.1 M Na_2SO_4	19.3 μg h^{-1} $mg^{-1}_{cat.}$	8.6	22
NbO_2 nanoparticle	0.05 M H_2SO_4	11.6 μg h^{-1} $mg^{-1}_{cat.}$	32	23
Cu-CeO_{2-x} nanorod	0.1 M Na_2SO_4	5.3×10^{-10} mol s^{-1} cm^{-2}	19.1	24
α-Au/CeO_x-RGO	0.1 M HCl	8.31 μg h^{-1} $mg^{-1}_{cat.}$	10.1	25
R-WO_3 nanosheet	0.1 M HCl	17.28 μg h^{-1} $mg^{-1}_{cat.}$	7.0	26
MoO_3	0.1 M HCl	29.43 μg h^{-1} $mg^{-1}_{cat.}$	1.9	27
d-TiO_2	0.1 M HCl	1.24×10^{-10} mol s^{-1} cm^{-2}	9.17	28

Table S2. The calculated zero-point energy (E_{ZPE}) and the product (TS) of temperature (T = 298.15 K) and entropy (S) of the different species along the reaction pathway on the catalyst, where * represents the adsorption site.

Species	E_{ZPE} (eV)	TS (eV)
N_2	0.15	0.58
*N-*N	0.21	0.09
*N-*NH	0.50	0.10
N-NH_2	0.86	0.10
N-NH_3	1.17	0.13
*N	0.08	0.04
*NH	0.35	0.07
*NH_2	0.70	0.07
*NH_3	1.02	0.13
*NH-*NH	0.82	0.11
NH-NH_2	1.18	0.13
NH_2-NH_2	1.53	0.15
NH_2-NH_3	1.73	0.20
NH_3-NH_3	2.04	0.26
1/2H_2	0.14	0.21
NH_3	0.89	0.60

References

1 D. Zhu, L. Zhang, R. E. Ruther and R. J. Hamers, *Nat. Mater*., 2013, **12**, 836–841.

2 G. W. Watt and J. D. Chrisp, *Anal*. *Chem*., 1952, **24**, 2006–2008.

3 P. E. Blöchl, *Phys. Rev. B*, 1994, **50**, 17953–17979.

4 G. Kresse and J. Furthmüller, *Phys. Rev. B*, 1996, **54**, 11169.

5 J. P. Perdew, K. Burke and M. Ernzerhof, *Phys. Rev. Lett.*, 1996, **77**, 3865–3868.

6 S. Grimme, J. Antony, S. Ehrlich and H. Krieg, J. Chem. Phys., 2010, **132**, 154104.

7 H. J. Monkhorst and J. D. Pack, *Phys. Rev. B*, 1976, **13**, 5188–5192.

8 J. K. Nørskov, J. Rossmeisl, A. Logadottir, L. Lindqvist, J. R. Kitchin, T. Bligaard and H. Jónsson, *J. Phys. Chem. B*, 2004, **108**, 17886–17892.

9 http://webbook.nist.gov/chemistry/.

10 S. Chen, S. Perathoner, C. Ampelli, C. Mebrahtu, D. Su and G. Centi, *Angew. Chem.*, *Int. Ed.*, 2017, **56**, 2699–2703.

11 X. Xiang, Z. Wang, X. Shi, M. Fan and X. Sun, *ChemCatChem*., 2018, **10**, 4530–4535.

12 Q. Liu, X. Zhang, B. Zhang, Y. Luo, G. Cui, F. Xie and X. Sun, *Nanoscale*, 2018, **10**, 14386–14389.

13 R. Zhang, X. Ren, X. Shi, F. Xie, B. Zheng, X. Guo and X. Sun, *ACS Appl. Mater. Interfaces*, 2018, **10**, 28251–28255.

14 X. Zhang, Q. Liu, X. Shi, A. M. Asiri, Y. Luo and X. Sun, T. Li, *J. Mater. Chem. A*, 2018, **6**, 17303–17306.

15 F. Wang, Y. Liu, H. Zhang and K. Chu, *ChemCatChem*, 2019, **11**, 1441–1447.

16 B. Xu, L. Xia, F. Zhou, R. Zhao, H. Chen, T. Wang, Q. Zhou, Q. Liu, G. Cui, X. Xiong, F. Gong and X. Sun, *ACS Sustainable Chem. Eng.*, 2019, **7**, 2889–2893.

17 Z. Wang, F. Gong, L. Zhang, R. Wang, L. Ji, Q. Liu, Y. Luo, H. Guo, Y. Li, P. Gao, X. Shi, B. Li, B. Tang and X. Sun, *Adv. Sci*., 2019, **6**, 1801182.

18 H. Huang, F. Gong, Y. Wang, H. Wang, X. Wu, W. Lu, R. Zhao, H. Chen, X. Shi, A. M. Asiri, T. Li, Q. Liu and X. Sun, *Nano Res.*, 2019, **12**, 1093–1098.

19 X. Wu, L. Xia, Y. Wang, W. Lu, Q. Liu, X. Shi and X. Sun, *Small*, 2018, **14**, 1803111.

20 L. Zhang, X. Ren, Y. Luo, X. Shi, A. M. Asiri, T. Li and X. Sun, *Chem. Commun*., 2018, **54**, 12966–12969.

21 K. Chu, Y. Liu, Y. Li, J. Wang and H. Zhang, *ACS Appl. Mater. Interfaces*, 2019, **11**, 31806–31815.

22 Y. Liu, Y. Li, H. Zhang and K. Chu, *Inorg. Chem.*, 2019, **58**, 10424−10431.

23 L. Huang, J. Wu, P. Han, A. M. Al-Enizi, T. M. Almutairi, L. Zhang and G. Zheng, *Small*

Methods, 2019, **3**, 1800386.

24 S. Zhang, C. Zhao, Y. Liu, W. Li, J. Wang, G. Wang, Y. Zhang, H. Zhang and H. Zhao, *Chem. Commun.*, 2019, **55**, 2952–2955.

25 S. Li, D. Bao, M. Shi, B. Wulan, J. Yan and Q. Jiang, *Adv. Mater.*, 2017, **29**, 1700001.

26 W. Kong, R. Zhang, X. Zhang, L. Ji, G. Yu, T. Wang, Y. Luo, X. Shi, Y. Xu and X. Sun, *Nanoscale*, 2019, **11**, 19274–19277.

27 J. Han, X. Ji, X. Ren, G. Cui, L. Li, F. Xie, H. Wang, B. Li and X. Sun, *J. Mater. Chem. A*, 2018, **6**, 12974–12977.

28 L. Yang, T. Wu, R. Zhang, H. Zhou, L. Xia, X. Shi, H. Zheng, Y. Zhang and X. Sun, *Nanoscale*, 2019, **11**, 1555–1562.